

# The Multi-Objective Adaptive Car-Following Control of Mengshi Intelligent Vehicle Based on Receding Horizon Optimization

Hongbo Gao<sup>1,2\*</sup>, Juping Zhu<sup>1</sup>, Fei Zhang<sup>3</sup>, Ruidong Yan<sup>4</sup>, Jianqiang Wang<sup>5</sup> & Keqiang Li<sup>5</sup>

<sup>1</sup>Department of Automation, University of Science and Technology of China, Hefei 230026, China;

<sup>2</sup>Institute of Advanced Technology, University of Science and Technology of China, Hefei 230088, China;

<sup>3</sup>Department of Computational Mathematics, School of Mathematical Sciences, Anhui University, Hefei 230601, China;

<sup>4</sup>School of Traffic and Transportation, Beijing Jiaotong University, Beijing 100044, China;

<sup>5</sup>School of Automotive Engineering, Tsinghua University, Beijing 100083, China

## Appendix A System Architecture of Mengshi Intelligent Vehicles

*Mengshi Intelligent Vehicle Hardware Architecture.* Mengshi intelligent vehicle are equipped with radar sensors, vision sensors and positioning sensors. The radar sensor includes the SICK LMS 291-S05 single-line laser radar, the IBEO LUX 4L laser radar, the IBEO LUX 8L laser radar and the Delphi ESR millimeter-wave radar. The vision sensor includes the AVT 1394 Pike F-100c camera. The positioning sensor includes the Global Positioning System (GPS) and Inertial Navigation System (INS) NovAtel SPAN-CPT. Mengshi intelligent vehicle and sensor installation location shown in Figure A1 and Figure A2, the sensor model, number, performance and usage have been shown in Table A1.



Figure A1 Mengshi intelligent vehicle.



Figure A2 Mengshi intelligent vehicle sensor mounting position.

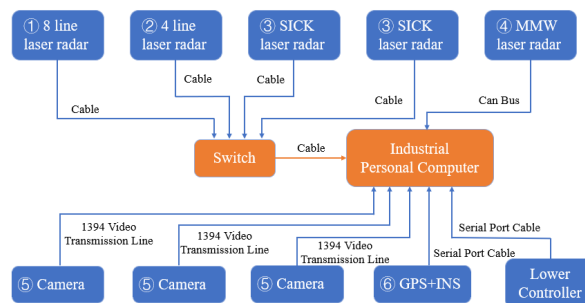


Figure A3 Mengshi intelligent vehicle hardware connection architecture

*Mengshi Intelligent Vehicle Hardware Connection Architecture.* The physical connection mode of the Mengshi intelligent vehicle sensor is shown in Figure A3 SICK LMS 291-S05 laser radar, IBEO LUX 4L laser radar and IBEO LUX 8L laser radar are connected to the computer through the virtual switch machine. But Delphi ESR millimeter-wave radar are connected to the computer directly through the CAN bus. GPS and INS are connected to computer through the COM line and AVT 1394 Pike F-100c

\* Corresponding author (email: ghb48@ustc.edu.cn, ghb48@ieee.org)

**Table A1** Mengshi intelligent vehicle sensor configuration

Sensor type	Num.	performance	Usage
IBEO LUX 8L	1	Range: 80m Angle: 180 DPI: 0.5 Period: 80ms	Road feasible area detection
IBEO LUX 4L	1	Range: 200m Angle: 110 DPI: 0.5 Period: 80ms	Pedestrian and vehicle detection
SICK Laser Measurement System (LMS)291-S05	2	Range: 80m Angle: 180 DPI: 0.5 Period: 80ms	Mid - range obstacle detection
Delphi Electronically System (LMS)291-S05	1	Range: 174m Angle: +/-10 DPI: 0.25 Period: 50ms	Long distance obstacle and Relative speed detection
AVT 1394 Pike-100c	3	DPI: 1000*1000 pixel Range: 80m Angle: 62.5 Period: 25-40ms	Traffic sign detection
NovAtel SPAN-CPT	1	Position DPI: 1cm Velocity DPI: 0.02m/s Pose accuracy: 0.05 degrees (pitch, roll) 0.1 degrees (azimuth) Frequency: 5Hz	Vehicle positioning, Vehicle attitude measurement and Vehicle acceleration

**Table A2** Nominal parameters of vehicle longitudinal dynamic model

parameters	Physical meaning	Unit	Nominal value
$\tau_e$	Engine time constant	$s$	0.3
$J_e$	Moment of inertia of crankshaft and pump wheel	$kg \cdot m^2$	0.28
$\eta_T$	mechanical efficiency	-	0.92
$i_0$	Transmission ratio of final drive	-	3.863
$M$	Equivalent vehicle mass	$kg$	1645
$r_w$	Tire rolling radius	$m$	0.301
$C_D$	Air resistance coefficient	-	0.37
$A_c$	Front face area	$m^2$	2.2
$g$	Acceleration of gravity	$m/s^2$	9.81
$f$	Rolling resistance coefficient	-	0.018
$K_b$	Braking system gain	$N \cdot m/MPa$	596.5
$\tau_b$	Braking system time constant	$s$	0.2
$\tau_d$	Braking system time lag	$s$	0.1
$k_q$	Dynamic fuel consumption compensation coefficient	$g \cdot s$	0.03

camera is connected to computer through the 1394 video transmission line. The information sensed by sensors is transmitted to the industrial computer through different transmission modes, and is processed to form planning and decision-making and transmitted to controller for controlling the accelerator, brake and direction.

*Experimental Environment and Vehicle Parameters.* The experimental environment of real vehicle in this paper is in normal traffic flow and good weather conditions, the maximum slope of the road is not more than 5%; Wind speed does not exceed level 4 ( $< 8m/s$ ); Good asphalt or concrete pavement, rolling resistance coefficient between 0.01 – 0.02, and combined with the technical parameters of the car itself, determine the nominal parameter value of the vehicle longitudinal dynamic model, as shown in Table A2.

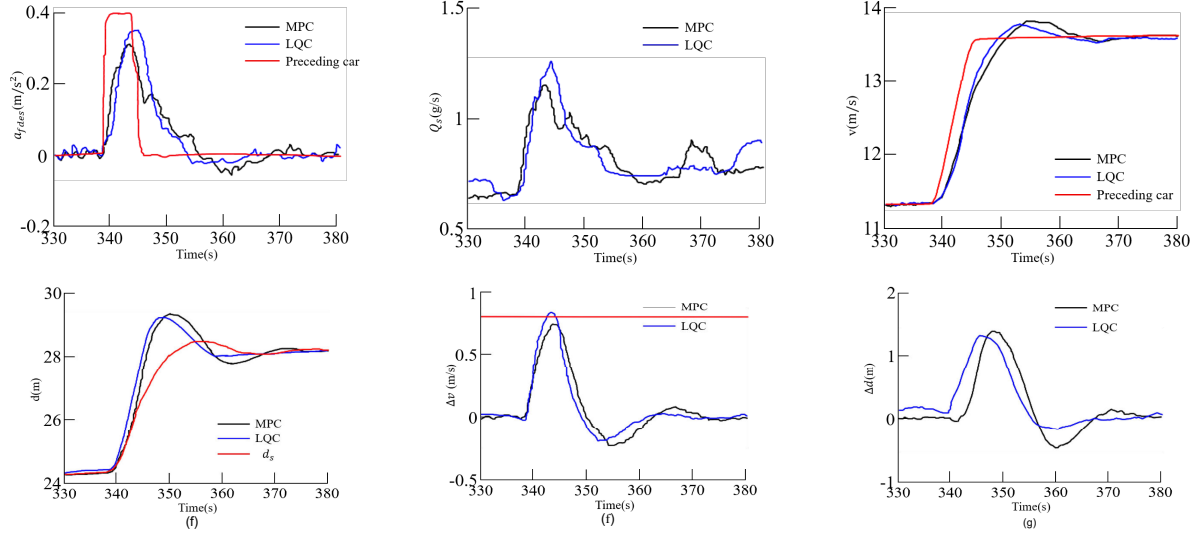


**Figure C1** The experimental results of urban road. (a) desired acceleration, (b) instantaneous fuel consumption, (c) vehicle speed, (d) Inter-vehicle distance, (e) relative speed, (f) vehicle distance error

## Appendix B LQC Algorithm for Performance Comparison

Because the Linear Quadratic Control (LQC) is a kind of multi-objective coordinated optimal control method which is suitable for linear objects. So the LQC method will be compared to receding horizon optimization method. According to the research achievements of Yi et al. [25], the controller design is the same, and the design of performance index is shown in (B1).

$$\int_0^{\infty} (x^T w_y x + u^T w_u u) dt, \quad (B1)$$

In (B1), in order to achieve the comparison result of LQC method and receding horizon optimization method, the weight coefficient of LQC method performance index is consistent with the weight coefficient of receding horizon optimization method in order to avoid the characteristic difference of control algorithm because of different parameters. The algebraic Riccati equation can be used to solve the linear feedback control law, as shown in (B2).

$$u = Kx, \quad (B2)$$

## Appendix C Experiment and Analysis of Urban Road

Figure C1 is the actual test results of the urban road conditions from 110 seconds to 160 seconds. (a) is the desired acceleration, (b) is the instantaneous fuel consumption, (c) is the vehicle speed, (d) is the Inter-vehicle distance, (e) is the relative speed, and (f) is the vehicle distance error. In Figure C1, the bold solid line represents the Mengshi intelligent vehicle receding horizon optimization method, the slender solid line represents the LQC method, and the dotted line represents the preceding vehicle state or the desired vehicle distance.

As can be drawn from Figure C1 (a), all of their acceleration meet the longitudinal ride comfort standard, but the acceleration of the receding horizon optimization method is more accurate to track the preceding vehicles acceleration, and its absolute value is lower than that of LQC method. The instantaneous fuel consumption curve of Figure C1(b) shows that the instantaneous fuel consumption of the receding horizon optimization method is lower than that of the LQC method in most time periods, indicating that the fuel economy of the former is better than the latter. As can be seen from Figure C1(c), (d), (e) and (f), the tracking speed and accurate of receding horizon optimization method is higher. And the relative vehicle speed and vehicle distance error are smaller than those of LQC method. These results show that the tracking performance of receding horizon optimization method is better than LQC method.

## Appendix D Experiment Results and Analysis of Expressway

Figure D1 is the real vehicle experimental data on highway conditions from 330 seconds to 380 seconds. (a) is the desired acceleration, (b) is the instantaneous fuel consumption, (c) is the vehicle speed, (d) is the Inter-vehicle distance, (e) is the relative speed, and (f) is the vehicle distance error. In Figure D1, the bold solid line represents the Mengshi intelligent vehicle receding horizon optimization method, the slender solid line represents the LQC method, and the dotted line represents the preceding vehicle state or the desired vehicle distance.

As can be drawn from the dashed line of Figure D1 (c), the preceding vehicle speed approximates speed step conditions during that period of time. Because the receding horizon optimization method has an acceleration detector of preceding vehicle, it can effectively detect the acceleration of the preceding car. The result of optimizing the performance index is to increase the acceleration of the vehicle as soon as it is, as shown at 340 to 342 seconds in Figure D1 (a). As can be seen from Figure D1 (c) and (d), because of the rapid increase in vehicle acceleration, receding horizon optimization method speed also increased fast from 340 seconds to 342 seconds, so that the distance between the vehicles will not be rapid expanded. Thus, after 342 seconds, although the maximum acceleration of the receding horizon optimization method is small, the relative vehicle speed is still less than the LQC method, and the vehicle distance error is not significantly deteriorated. In Figure D1 (b), the instantaneous fuel consumption of the receding

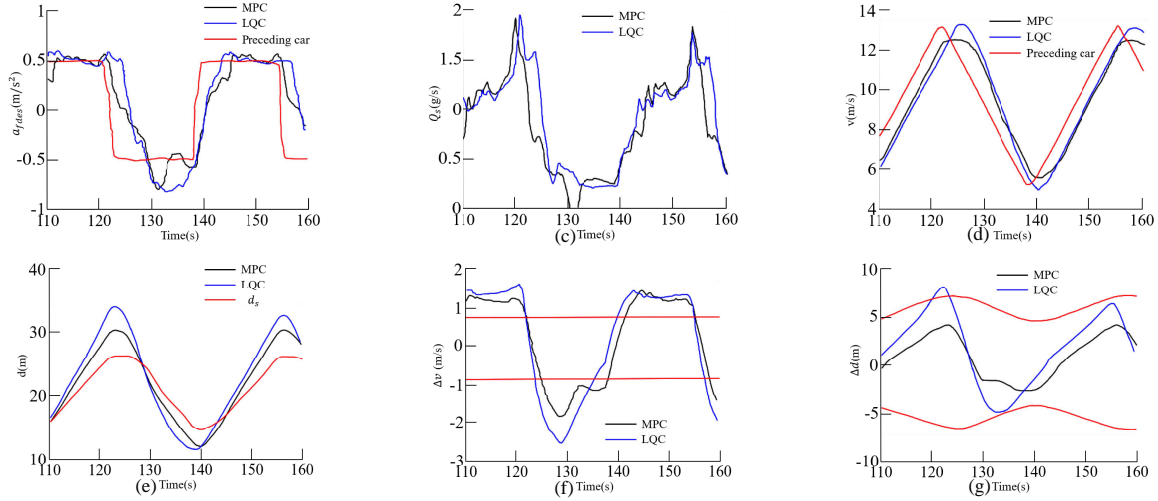


**Figure D1** Experimental results of expressway. (a)desired acceleration, (b)instantaneous fuel consumption, (c)vehicle speed, (d)Inter-vehicle distance, (e)relative speed, (f)vehicle distance error.

horizon optimization method also increases rapidly, but the maximum value of instantaneous fuel consumption is less than that of the LQC method, which is consistent with the change trend of acceleration.

## Appendix E Comparative Analysis of Fuel Economy and Tracking Performance

The fuel economy of the receding horizon optimization method for the Mengshi is evaluated. The Fuel Consumption per Hundred Km (FCH) is used as the fuel economy evaluation index, as shown in (E1).

$$FCH = 100 \frac{\rho g \sum_{i=1}^N Q_s(i) T_s}{\sum_{i=1}^N v_f(i) T_s}, \quad (E1)$$

In (E1),  $\rho$  is the density of gasoline. The value is  $0.72510 - 3L/g$ ,  $N$  is number of data of the experimental process,  $Q_s$  is the instantaneous fuel consumption, the unit is  $g/s$ .

To evaluate the tracking performance of the receding horizon optimization method of the Mengshi, the Track Error Index (TEI) was taken as the tracking performance index, as shown in (E2).

$$TEI = \frac{1}{N} \sum_{i=1}^N (|\Delta v_i \cdot SVE| + |frac{\Delta d(i)}{SDE} \cdot SDEK_{TE}|), \quad (E2)$$

In (E2),  $\Delta v$  is the relative speed,  $\Delta d$  is the Inter-vehicle distance error, SVD/SDE is the driver's sensitivity model of tracking error, and  $K_{TE}$  is the coefficient of the two-dimensional distribution model, which is 8.42.

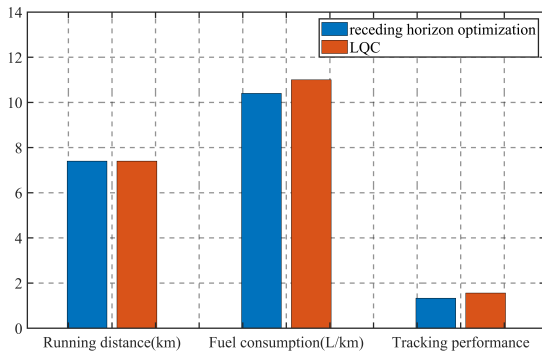


**Figure E1** Comparison of fuel economy and tracking performance of urban road conditions.

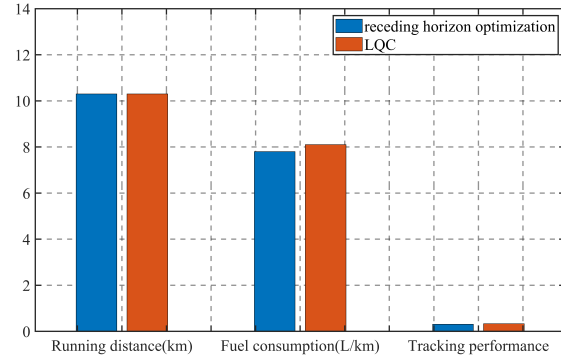


**Figure E2** Comparison of fuel economy and tracking performance of expressway conditions.

The experimental data in sections 6.3 and 6.4 are analyzed. The FCH and tracking performance of the receding horizon optimization method and the LQC method are calculated using equation 31 and equation 32, respectively, as shown in Figure E1 and Figure E2. As can be seen from Figure E1, the FCH of receding horizon optimization method was reduced by 5.3% than that of LQC method. The tracking error index reduced by about 14.9%. As can be seen from Figure E2, FCH of receding horizon optimization was reduced by 2.5% than that of LQC method. Tracking error index reduced by about 1.8%. As a result, the receding horizon optimization method can improve the performance fuel economy and tracking of intelligent vehicles at the same time.